Consistency of rocket and radar electron density observations: implication about the anisotropy of mesospheric turbulence

B. INHESTER,* J. C. ULWICK,† J. CHO,‡ M. C. KELLEY‡ and G. SCHMIDT*

* Max-Planck-Institut für Aeronomie, D-3411 Katlenburg-Lindau, F.R.G.; † Department of Electrical
Engineering, Utah State University, Logan, Utah, U.S.A.; ‡ Department of Electrical Engineering,
Cornell University, Ithaca, New York, U.S.A.

Abstract—We report about a quantitative comparison of rocket observations of electron density fluctuations and simultaneous 53.5 MHz radar measurements that were obtained during the MAC/SINE campaign in northern Norway in summer 1987. Out of three rockets launched during the Turbulence/Gravity Wave salvo on 14 July 1987, two were flown during conditions that allowed a detailed investigation. For a large part of the data from these rocket flights it is found that the radar reflectivity is about 10 dB, enhanced over what would be expected from the rocket observations in the case of isotropic electron density fluctuations. The observations can be reconciled under the assumption of an anisotropic turbulence. Assuming a simple model spectrum for the electron density fluctuations, we derive a relation between the rocket and radar observations that covers the whole range from isotropic turbulent scatter to Fresnel scatter at horizontal density stratifications. For the observed dataset, an anisotropy which typically corresponds to a ratio of the horizontal to the vertical coherence length of about 10 is consistent with the comparison of rocket and radar observations. A similar anisotropy is found also from the observed aspect sensitivity of the radar echoes. The variation of the anisotropy with height and time shows an anticorrelation with the turbulence level of the mesosphere as deduced from the spectral width of the radar echoes. The anisotropy is found to maximize in heights where the electron density displays deep 'bite-outs'. These depletions in the electron density were independently observed by a Langmuir and an admittance probe on board two of the rockets.

1. INTRODUCTION

In this paper, we report about the comparison of a series of *in situ* rocket-borne electron density measurements with simultaneous radar observations during the Turbulence/Gravity Wave salvo of the MAC/SINE campaign. Such comparisons of ion or electron density measurements in the upper mesosphere on board rockets with ground-based radar observations have first been carried out by THRANE *et al.* (1981) and HOCKING and VINCENT (1982) using radars at transmission frequencies in the MF/HF frequency range. However, a quantitative comparison of the electron density fluctuations with radar echoes at these frequencies turned out to be difficult because radar waves at such low frequencies are subject to substantial *D*-region absorption and refraction. Moreover, these radar systems are difficult to calibrate. Nevertheless, it could be concluded from these studies that turbulent scatter (THRANE *et al.*, 1981; ROYRVIK, 1985) and quasi-specular reflection (HOCKING and VINCENT, 1982) were both important scattering mechanisms for mesospheric radar echoes at MF/HF frequencies.

Similar experiments have been repeated later by ROYRVIK and SMITH (1984) at low latitudes and by ULWICK *et al.* (1988) in the polar summer mesosphere. The latter experiment was carried out as a part of the STATE campaign which took place at Poker Flat, Alaska, in summer 1983. The above authors used rocket-borne Langmuir probe observations to compare with mesospheric radar echoes at 50 MHz. In both of these experiments, the mesospheric radar scatter was assumed to be caused by turbulent and isotropic electron density irregularities. ROYRVIK and SMITH (1984), however, utilized a radar with a poor range resolution so that only an order of magnitude comparison between the observed echo intensity and the estimated intensity from the rocket probe measurements was possible. They found consistency with their assumptions within these coarse error bounds. In the detailed comparison by ULWICK *et al.* (1988) a good quantitative correspondence of the height profiles of the measured electron density irregularities and the backscattered radar returns was obtained in the height range between 80 and 90 km. However, in the height of the power maximum, the echo power estimated from the rocket measurements was systematically larger than the echo power observed in a 15° off-zenith beam direction if isotropy

of the electron density irregularities was assumed.

In the recent past, evidence has grown from vertical and oblique radar observations that the scattering electron density irregularities at upper mesospheric heights are at least temporarily not isotropic even at VHF wavelengths (FUKAO et al., 1979; CZECHOWSKY et al., 1988). Moreover, it is difficult to understand why the horizontally stratified scattering layers that are inferred from the HF radar observations and that are sometimes assumed to have a vertical scale size of only some 10 m should not have any influence on the irregularities at VHF scattering lengths of about 3 m. Some indirect evidence of these stratified density irregularities can also be found in the electron density spectra observed by rocket probes. At least for one of the rocket flights during the STATE campaign the obtained spectra show indications of a k^{-2} wave number range at wavelengths above some meters, which are reminiscent of vertical electron density steps (KELLEY and ULWICK, 1988). The energy cascade intimately connects the energy spectral density at all scales of the buoyancy and the inertial range. As the electron density largely behaves as a passive tracer in the turbulent motion of the neutral air, a similar interdependence of different scales can be expected to exist for the electron density fluctuation spectrum. Consequently, only a gradual change from the predominant horizontal stratification at larger wavelengths to isotropy at small wavelengths should occur.

It must be stressed that both the radar and the rocket probes can see mesospheric turbulence only indirectly by means of the electron density fluctuations. The link between turbulence and density fluctuations is provided by the widely accepted assumptions that the mesospheric ions can be considered as a passive tracer (HILL and BOWHILL, 1976; THRANE and GRANDAL, 1981), and that the electron charge density screens the ion density to maintain quasi-neutrality. The latter assumption is certainly satisfied at scales longer then the Debye length of the plasma, while the first assumption loses its validity somewhere at very large scales for which the eddy turnover time exceeds the lifetime of the ions. HILL and BOWHILL (1976) estimate their lifetime in the mesosphere to be longer than 100 s. For scales of the order of the radar wavelength that are of interest here, the first of the above assumptions is therefore very likely to hold because the typical autocorrelation time of mesospheric 3-m irregularities as inferred from the width of the radar signal is only of the order of 1 s or less.

In order to understand turbulent transport and dissipation in the upper atmosphere, a quantitative mea-sure of the anisotropy of the electron density irregularities at various length scales would be desirable. In the present work, we attempt to determine a parameter that measures the anisotropy of mesospheric turbulence both from the radar aspect sensitivity and from the comparison of the radar and rocket observations. The paper is organized as follows: in Section 2 we explain some experimental details and the geometry of our experiment, in Section 3 the experimental results of the rocket and radar observations are presented and are quantitatively compared in Section 4, and a final discussion and summary is presented in Section 5.

2. EXPERIMENTAL SET-UP

As part of the MAC/SINE campaign, four Super ARCAS rockets were launched from the Andøya Rocket Range, Andenes, Norway, on 14 and 15 July 1987. Among these four rockets, three were dedicated to study mesospheric turbulence and gravity waves in a joint observation on 14 July over a time period of several hours together with ground-based and other rocket measurements (Turbulence/Gravity Wave salvo). The fourth rocket was launched on 15 July 1987 when in addition to other ground-based facilities, the EISCAT radar was operating (EISCAT salvo). The results of this latter experiment will be reported elsewhere (KELLEY et al., 1990).

All four Super ARCAS rockets had simple d.c. probes (Langmuir type) for the measurement of electron currents at high resolution, as were flown on the STATE rockets (ULWICK et al., 1988). The relative electron density was measured by monitoring d.c. electron current to the isolated tip of the nose cone, which was held at a fixed $+3$ V bias potential with respect to the rocket skin. The collected current was converted to a 16-bit digital number and transmitted to the ground at a rate of 8000 bytes/s. This gives excellent data to carry out power spectral analysis, but does not give absolute electron density necessary for calculating the radar reflectivity from the rocket data. Furthermore, the STATE data revealed electron depletions in the intense backscatter regions, including for STATE 3 a deep 'bite-out' in the electron density of more than an order of magnitude. To determine to what extent the electron depletions were real, two of the MAC/SINE Super ARCAS rockets had, in addition to the d.c. probe, an RF capacitance probe for the measurement of absolute electron density. This probe has been used in several mesospheric investigations (e.g. HARRIS et al., 1983), and details of a description of the probe are contained in this reference. Briefly, an RF generator generates 3.0 MHz and the oscillator output is fed

through an RF bridge to one-half of the instruments dipole antenna and the guard electrode. The ground return for this dipole is the Super ARCAS rocket body. When immersed in the ionospheric plasma, the dipole can be equated to a simple parallel RC circuit with values of R and C dependent upon electron density of the ionospheric medium. As these values change due to changes of electron density of the plasma, imbalances in the RF bridge circuitry result. These changes are amplified and synchronously detected, and are commutated to form the output of the probe. We only flew the RF probe on two of the rockets because of concern that this 'heavy' payload's apogee would be marginal relative to the peak altitude of the intense backscatter region near 90 km. However, all rockets reached altitudes above 93 km with the peak altitude more dependent of winds than the extra 2 lb. of weight of the 'heavy' payload. In the next section the probe measurements are compared and discussed; the value of adding the RF probes is clear and any future flights will have both probes.

During the time of the rocket launches and in between, the mobile SOUSY-VHF radar system was operated at 53.5 MHz in a 6-beam mode looking sequentially into the vertical, towards NE, NW and SW with a $4°$ angle and towards N and W at a $5.6°$ angle off-zenith. The integration time for each single beam measurement was about 10 s, so that a full beam cycle took about 1 min. The range resolution was $\Delta r = 300$ m and a height range from 60 to 100 km was covered. The radar was operated at a peak transmitter power of $P_t = 75$ kW, which is about half the maximum possible power. The low power mode was chosen in order to reduce the possibility of a transmitter failure during its continuous operation for the time of the MAC/SINE campaign of more than a month. A list of the other radar parameters and a further description of the radar system can be found in CZECHOWSKY et al. (1984).

The radar receiver was calibrated both by a noise source of known temperature (varied between 0 and 12,000 K) and independently by an attenuated transmitter signal that was directly fed into the receiver after measuring its amplitude. Both methods gave results consistent within 10%, the error probably being due to the uncertainty with which the receiver bandwidth is known. The calibration was repeated for another radar program with a different code, pulse length etc., and a deviation of the calibration constant of only 20% was found if the effects of coding, pulse length and attenuation were accounted for (HOCKING et al., 1983). This calibration procedure enabled us to convert the received power P_r from tape units to physical units so that we did not have to guess the

noise power and then use the signal-to-noise ratio to infer the received power. The noise power P_n is essentially due to galactic and instrumental noise and the first of these noise sources varies appreciably in Andenes by more than a factor of 2 within a sideral day. This makes signal-to-noise ratios difficult to compare during the course of the day.

The noise power is needed here only for subtraction from the received power. This difference, the echo power $P_r - P_n$ from a distance r is often expressed in terms of a radar reflectivity η_{radar} (BATTAN, 1973)

$$\eta_{radar} = 8 \frac{r^2 k_{radar}^2}{G \Delta r} \cdot \frac{P_r - P_n}{\alpha P_t} \tag{1}$$

where $k_{radar} = 1.12$ rad/m is the radar wave number of the SOUSY system, $G = 10^{3.55}$ is its antenna gain, and α takes account of losses on the transmission and receiving path of the radar system (of about 3 dB for the SOUSY radar). For a typical noise power, a 1 dB signal-to-noise ratio with $P_r = 2P_n$ from a height of 85 km yields for the SOUSY parameters a reflectivity of about $6.5 \cdot 10^{-17}$ m^{-1}. In physical terms, η_{radar} is 4π times the differential backscattering cross-section of a unit volume. Equation (1) assumes that the total radar volume contributes homogeneously to the scattered signal (volume-filled scattering). The radar volume at a distance r is $\frac{1}{2}\Omega r^2 \Delta r$, where $\Omega = 4\pi/G$ denotes the solid angle of the antenna beam characteristic. The horizontal extent of the radar volume in a height of 85 km is about 4 km in diameter. One of the fundamental assumptions upon which the interpretation of our observations is based is the statistical homogeneity of the electron density turbulence over at least the scale size of the radar volume.

In the left part of Fig. 1 the geometry for the experiment at the Andøya Rocket Range is shown. The rocket launch site is at the origin and an arrow shows the general azimuth of the Super ARCAS launches, with a legend giving the approximate range and altitudes of the rockets at various points along the ground track. The location of the SOUSY radar is shown along with the azimuths for its five off-zenith beams and the intersection of these beams with a plane in an altitude of 85 km, where echoes most probably occur during the summer. The data obtained during the ascent of the rocket flight were thus obtained about 20 km north and 5 km east of the closest SOUSY beam (north beam). The velocity of the rocket at a height of 85 km was about 450 m/s during the ascent and the velocity vector made an angle of roughly $30°$ with the vertical in this height. The right part of the figure shows a sketch of the beam and rocket geometries as another perspective.
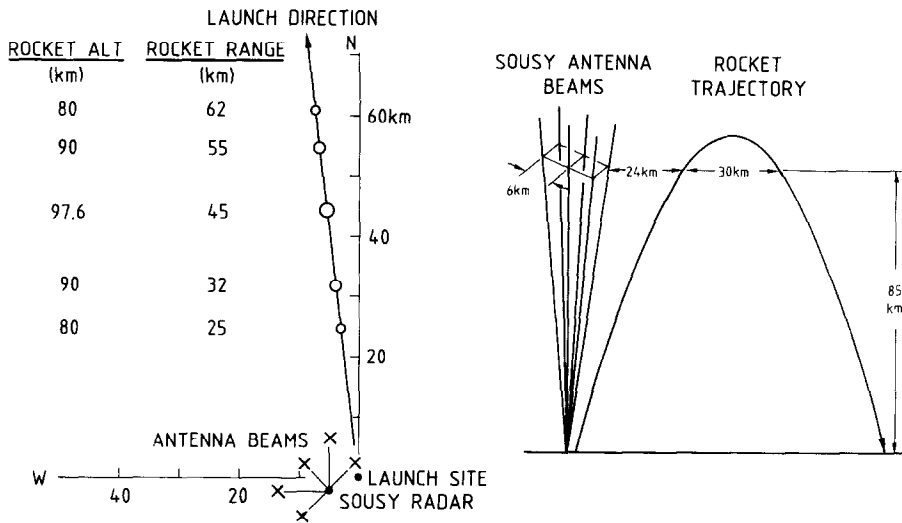
Fig. 1. Sketch of the relative location of the Super ARCAS rocket trajectories and the SOUSY antenna beams. There are six antenna beams of the SOUSY radar pointing vertically, towards NE, NW and SW with 4° off-zenith angle and towards N and W with 5.6° off-zenith angle. The left part of the figure is a view from the top. The crosses denote the horizontal coordinates of the radar beams at a height of 85 km; the open circles give the rocket position at the indicated height. The right part of the figure shows a side view of the beam configuration and the rocket trajectory.

3. EXPERIMENTAL RESULTS

The three Super ARCAS rockets dedicated to the Turbulence/Gravity Wave (TGW) salvo were launched on 14 July 1989 at 0800, 0929 and 1255 UT. In the following, we shall briefly refer to these launches by their sequence number 1, 2 and 3, respectively. In Fig. 2 we show the echo power obtained for the vertical beam of the SOUSY radar during this time interval. The rocket launches are indicated by a vertical vector above the time axis. At the beginning of the time interval, between 7 and 8 UT, there was substantial backscatter of more than 40 dB above the noise. The backscatter intensity then declined steadily until it almost disappeared entirely after about 12 UT. The high echo intensity fingers pointing downwards in time from the bottom side of the echo layer between 8 and 10 UT are probably indications of gravity waves propagating from below (FRITTS et al., 1988).

3.1. Rocket probe results

The d.c. (Langmuir type) probe has been used extensively in research studies on the ionization in the upper atmosphere. It has been shown to be especially useful in investigations of electron density structure in the F-region (e.g. SZUSZCZEWICZ et al., 1980; KELLEY et al., 1982), in the E-region (e.g. PRAKASH et al., 1972; PFAFF et al., 1982), in the mesosphere (e.g.

ROYRVIK and SMITH, 1984; ULWICK et al., 1988) and in barium clouds (BAKER and ULWICK, 1978). However, it is common to calibrate the d.c. probe using some other form of electron density measurements because no satisfactory method is available to derive the electron density from the fixed-bias d.c. probe collected current. There is a danger in this, as pointed out by BAKER et al. (1985), because the sensitivity of the Langmuir probe depends quadratically on the Debye length. In MAC/SINE one of our objectives was to determine the extent and limitations of using the fluctuations $\Delta I/I$ in the current to derive electron density scale lengths and fluctuation levels $\Delta N_e/N_e$ in the mesosphere. Therefore, two of the rockets were flown with an added RF capacitance probe. The second and third rockets of the TGW salvo were chosen to provide consecutive measurements of an intense backscatter region decaying to a low or no backscatter situation.

Figure 3a shows the superposition of the RF probe electron densities on the densities derived from the d.c. probe currents for the second rocket flight. The attempt is to achieve the best fit to the results above and below the region of electron depletion. Except for the depletion region there is surprisingly good agreement in the two profiles, even in fine scale structure in the mesosphere region, i.e. below 90 km. Above
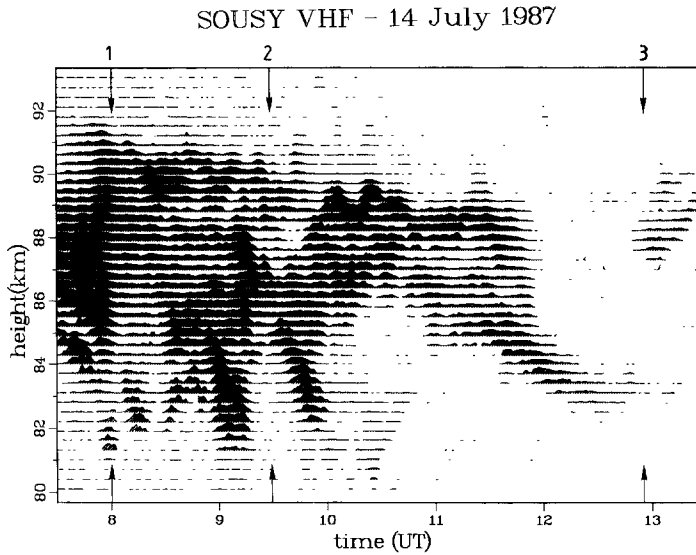
SOUSY VHF — 14 July 1987

Fig. 2. Relative echo intensity observed in the vertical SOUSY beam during the time of the Turbulence/Gravity Wave salvo. The distance from one range gate to the next is 300 m. The height of the grey-shading within each range gate is proportional to the logarithm of the echo intensity in the height such that a grey-shading over a full range gate corresponds to a signal-to-noise ratio of 40 dB. The launch times of the Super ARCAS rockets are indicated by arrows above the abscissa.

90 km the electron density derived from the d.c. probe currents becomes progressively less than the electron density inferred from the RF probe. This discrepancy is most likely due to spin-related wake effects or changing Debye shielding effects (BAKER et al., 1985). In the region of electron depletion from about 82 to 88 km, the d.c. probe indicates a smaller electron density than the RF probe. The d.c. probe results are reduced in a nonlinear fashion with the largest deviation at the 'bite-out' in the electron density at 86 km. KELLEY and ULWICK (1988) suggested the presence of heavy water cluster ions in this uniquely cold region of the atmosphere to explain the intense summer radar echoes. This suggestion is supported by the fact that these ions are known to sometimes form sharp density gradients in the mesopause region, their appearance is favored by small electron densities as they exist inside the 'bite-outs' (e.g. REID, 1989), and they are supposed to enhance the backscatter by reducing the ion density diffusion (KELLEY et al., 1987). The presence of the water cluster ions may also be related to the lower relative current readings in the 'bite-out' region. At the moment, however, we cannot rule out the presence of other positively charged heavy ions or dust particles to account for the anomalous d.c. probe response inside the 'bite-out' or the effect of payload charging. These possibilities will be studied further in a future publication.

In Fig. 3b, the RF probe electron densities from the ascent of the third rocket flight are superimposed on the d.c. probe densities to obtain the best fit to the data above and below the depletion region, as was done for the second flight. The results show a small 'bite-out' in the electron density profile of about 10% and in the d.c. probe densities of about 35% at 82 km. Above this region up to a height of 88 km the RF probe electron density is slightly higher than the d.c. probe density by an almost constant factor. Overall, however, there is very good correspondence between the RF and d.c. density profiles as in the results of the second flight. Furthermore, the correction factor to change the d.c. probe currents to electron densities is almost identical for both flights, which is also very encouraging. Therefore, we will use this constant factor, 4.5×10^9 electrons/(cm^3 ampere), to obtain the electron density from the d.c. probes for the profiles of the first rocket of the TGW salvo presented in this paper, and also for those from the rocket launched at the EISCAT day on 15 July 1987 (KELLEY et al., 1990). For the depletion regions a first-order empirical correction factor will be invoked when electron densities are required in the calculation of the radar reflectivity from the rocket probe measurements.

We often observe that the d.c. probe currents near the peak of the trajectory and on rocket descent are smaller than the ascent values, presumably due to
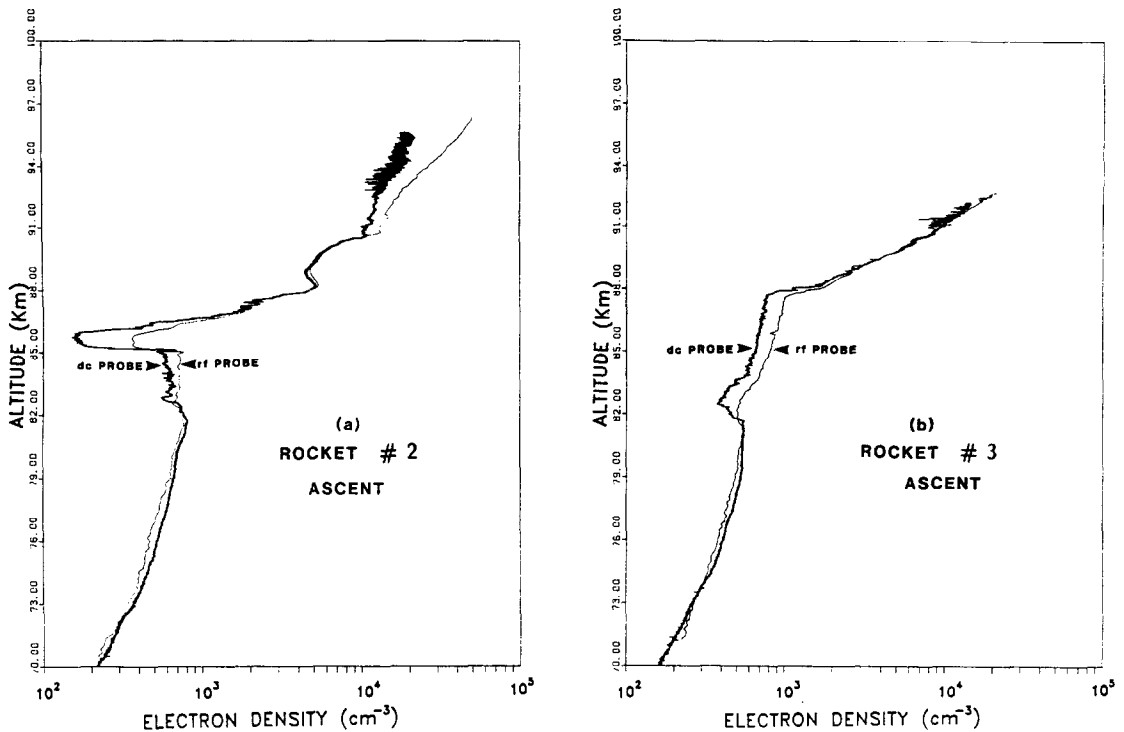
Fig. 3. Superposition of the d.c. probe electron currents to a best fit to the corresponding electron densities from the RF probes for the second (a) and third (b) rocket flight of the TGW salvo. The resulting conversion factor to obtain the electron density from the d.c. probes is 4.5×10^9 electrons/(cm^3 ampere) and is nearly identical for both rockets.

spin/wake effects. This effect exists until aerodynamic torque causes the spacecraft to tip over and align with the velocity vector rocket tip near 80 km. Our experience with RF probe measurements, however, shows no such effect for these types of probes. This is shown in Fig. 4a,b, where we have overlaid the descent results on the ascent results for both rockets. Note that although the ascent results are higher than the descent results near 88 km for both flights, above and below this region there is good agreement. The agreement also includes the structured 'bite-out' regions which are horizontally separated by more than 35 km. For the second rocket there is an added 'bite-out' region near 83 km on rocket descent not present in the ascent results. This, however, is the same altitude of the 'bite-out' shown in the results from the third rocket obtained about 3.5 h later. These data show that at vertical scales of a few kilometers some features are similar over horizontal separation distances of tens of kilometers indicating a horizontal coherence length of at least 10 times the vertical co-

herence length for these density structures. At vertical scales of meters, however, features are not the same between the ascent and descent of the rocket trajectory.

3.2. Rocket–radar comparison

The comparison between the ascent rocket electron density profiles and the radar cross-sections for the north beam, which is the closest SOUSY beam, is presented in Fig. 5 for the TGW salvo. The EISCAT salvo results are also shown in Fig. 5d for comparison purposes. As noted above, the electron density profiles were obtained from the d.c. probe that was calibrated using the RF capacitance probe measurements. The radar reflectivity is the result of an averaging over three records (= 3 min) centered around the time shown. In Fig. 6 we present the square of the spectral width of the radar returns from the vertical beam for about the same instances, although averaged over 10 min to give more reliable estimates.

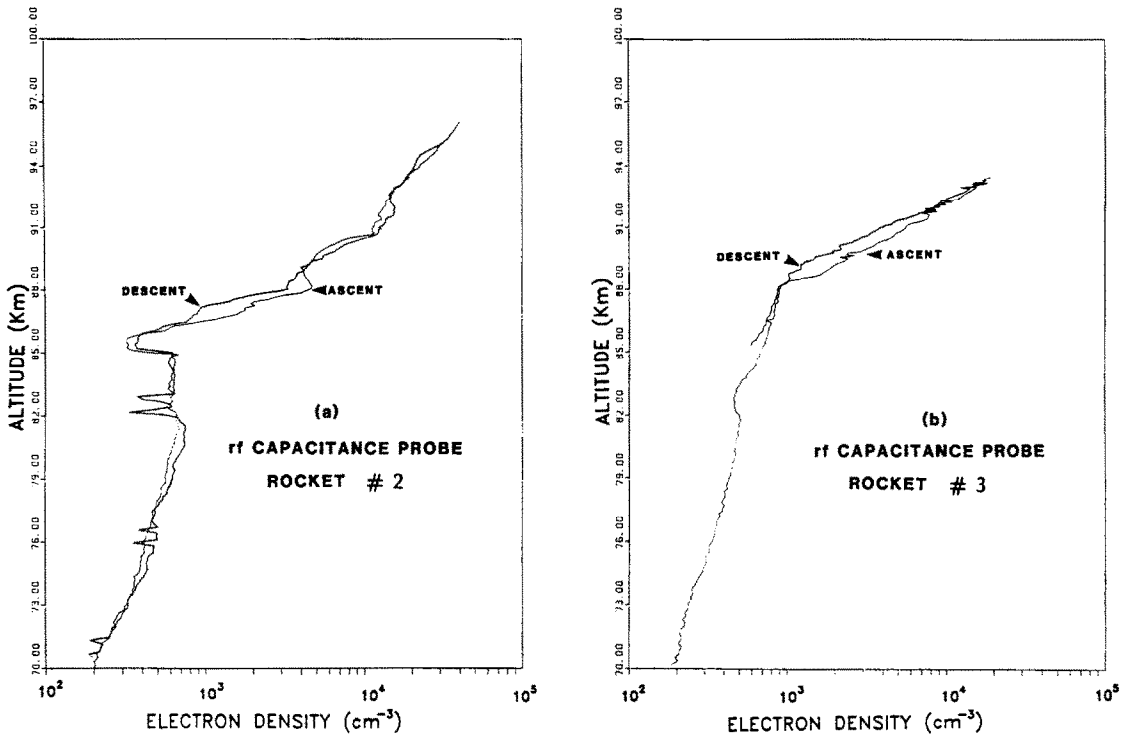In general, the large fluctuations and strong gradi-

Fig. 4. Comparison of the rocket ascent and descent RF probe electron density results for the second (a)
and third (b) rocket flight of the TGW salvo.

ents in electron density occurred in the regions of most intense backscatter. This was also true for the two STATE rocket measurements. It is obvious that the radar reflectivity on the EISCAT day was much stronger (by more than one order of magnitude) than the highest measured reflectivity on the TGW day. However, equally obvious is that the electron density in the peak scattering region during the EISCAT rocket flight was about an order of magnitude greater than during the TGW event. Such variations in D-region electron density are quite interesting and may be caused by a combination of enhancements due to particle precipitation and changes in recombination rates due to the formation of cluster ions. The EISCAT rocket electron density profile and that of the first rocket flight on TGW day are characterized by highly variable or 'turbulent' fluctuations similar to the STATE 1 results. As shown in Fig. 6a, the vertical velocity fluctuations are substantial at that time in the whole height range between 80 and 90 km. The same holds true for the fluctuations during the EISCAT day flight (KELLEY et al., 1990).

The second TGW rocket electron profile, on the other hand, is very similar to the STATE 3 results in that the region of radar backscatter partly corresponds to the altitude of steep gradients in the electron density caused by a deep 'bite-out' in the electron density of almost an order of magnitude. The lower of the two echo layers that formed at 0930 UT seems to be associated with this 'bite-out' observed just above 85 km. The vertical velocity fluctuations (Fig. 6b) have a marked minimum at that height so that the scattering mechanism is either quasi-specular reflection or some chemical processes give rise to both the electron 'bite-out' and the backscatter intensification as proposed by KELLEY and ULWICK (1988). As mentioned above, the different response of the d.c. and RF rocket probes to the 'bite-out' may be taken as an indication of such chemical processes. The second echo layer at slightly below 90 km seems in the reverse to be associated with strong vertical velocity fluctuations comparable to the 'turbulent' fluctuations observed during the first rocket flight.

The third TGW salvo rocket results show only a small depletion (about 10%) near 83 km which corresponds to a small backscatter signal just above the
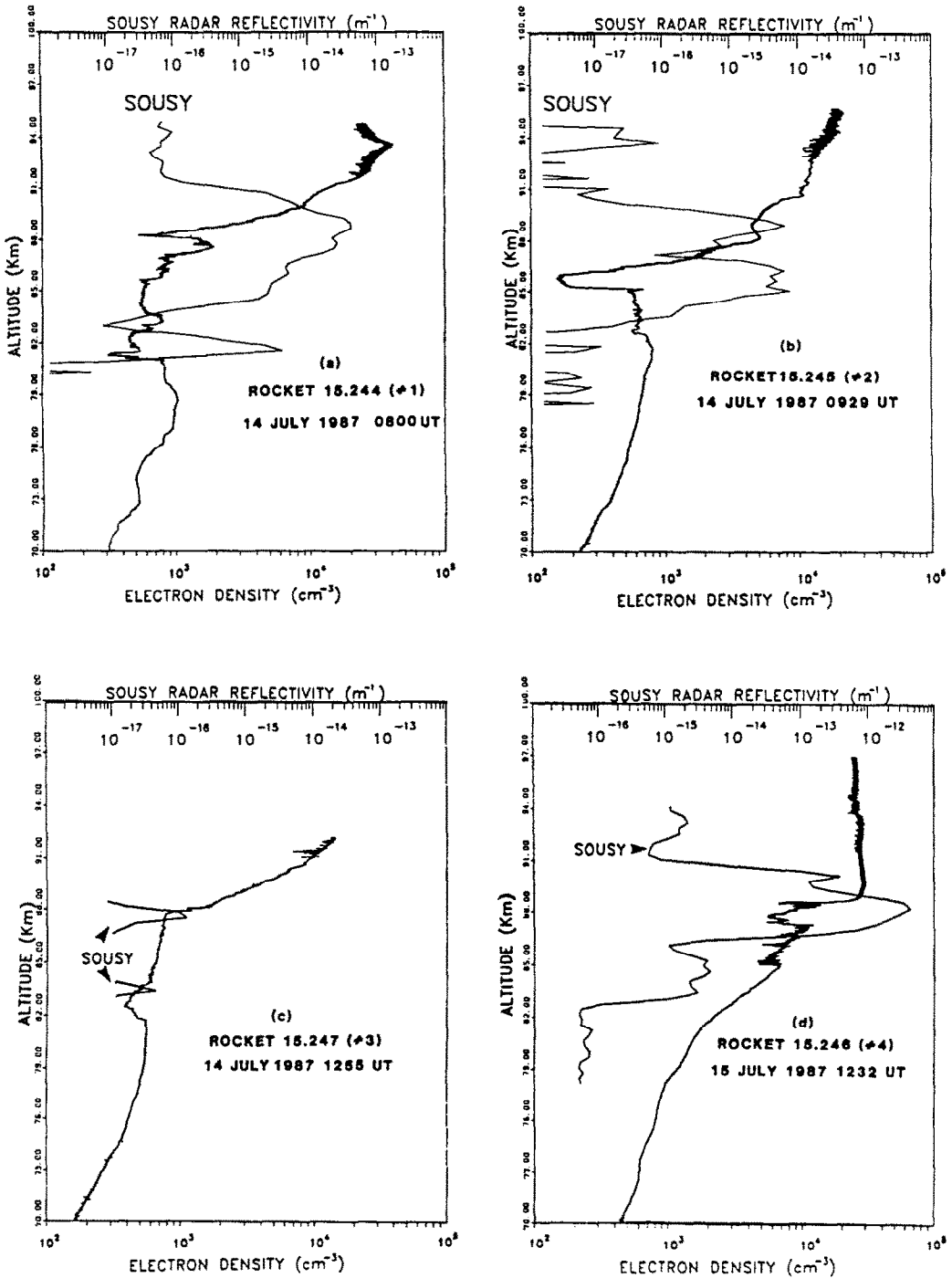
Fig. 5. Comparison of the ascent rocket electron density profiles from the d.c. probes and the SOUSY radar reflectivity observed simultaneously in the northward beam for the four MAC/SINE rockets. The panels (a)–(c) show the results of the TGW salvo flights No. 1–3, respectively; panel (d) displays the results of the EISCAT salvo.
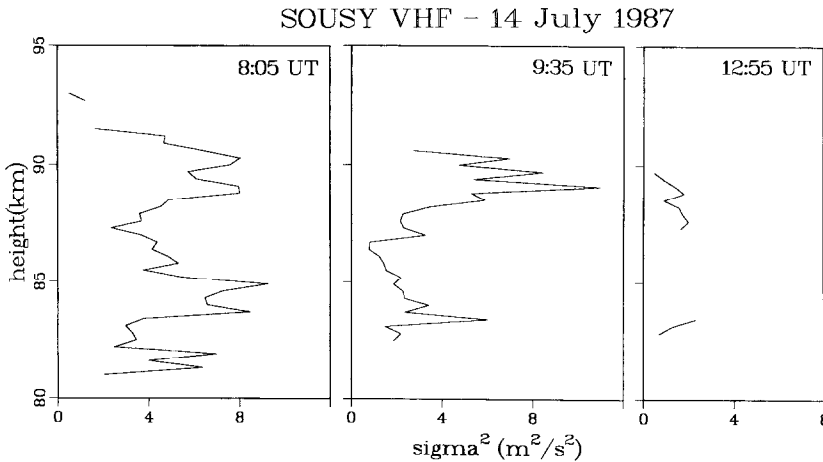
SOUSY VHF – 14 July 1987

Fig. 6. Height profiles of the squared spectral width of radar signal observed in the vertical beam during the TGW salvo rocket flights. The values are averaged over 10 min centered around the times indicated.

noise level. Above about 89 km there are some small-scale structures which give rise to somewhat stronger echoes. Neither the processes forming the 'bite-out' nor the vertical velocity fluctuations are obviously sufficient to produce remarkable backscatter at 1250 UT.

In order to quantitatively compare the rocket observations of the small-scale density fluctuations and the radar reflectivity, we use the same approach as with the STATE results, i.e. we power-spectrally analyze the probe data and use the formula given by ROYRVIK and SMITH (1984) to obtain equivalent reflectivities η_{rocket} based on the assumption that the observed electron density fluctuations are isotropic. The relation used by ROYRVIK and SMITH [1984; equation (6)] can be written as

$$\eta_{\text{rocket}}(k_{\parallel}) = n8\pi^3 \left(\frac{r_e}{k_{\parallel}}\right)^2 S_N(k_{\parallel}) \qquad (2)$$

where $r_e = 2.82 \cdot 10^{-15}$ m is the classical electron radius and

$$S_N(k_{\parallel}) = \frac{V}{\pi T} \left| \int_T dt \delta N_e(t) \, e^{ik_{\parallel}Vt} \right|^2 \qquad (3)$$

is the power spectral density of the electron density fluctuations δN_e at wave number $k_{\parallel}$ along the rocket trajectory, n is the spectral index of S_N, V is the rocket velocity and T the length of the time interval considered for the power spectral estimation. Here, VT was chosen such that a spatial resolution comparable to the radar range resolution of 300 m was obtained. The probe data from the first two rockets in the TGW salvo were analyzed, but not the third, because the

echoes were too weak at that time. For the second rocket we used the absolute electron densities from the RF probe and the spectra from the d.c. probe. For the first rocket the calibration of the d.c. probe was used as previously described.

The results of the analysis for $k_{\parallel}$ equal to the SOUSY scattering wave number of $2k_{\text{radar}} = 2.24$ rad/m are given in Fig. 7a,b, along with the SOUSY results for the north beam. For the first rocket (Fig. 7a) there is agreement between the rocket and radar results concerning the general variation of the reflectivity with altitude, except that the rocket results appear slightly compressed and downshifted in height. Also, the peak of the calculated rocket reflectivity indicates much more structure than observed by the radar. The maximum values of η_{rocket} and η_{radar} are in approximate quantitative agreement, even though they are at slightly different heights at 87.5 and 89 km, respectively. Above and below these heights, however, the rocket reflectivity seems to decline much more rapidly than the reflectivity observed by the radar, the discrepancy reaching an order of magnitude below the peak and even more so above. The observations in the height region below 84 km are difficult to compare because there is a significant spatial and/or temporal structuring of the electron density at that time. Referring back to Fig. 2, we note that the radar return from around 82 km only lasts for about 5 min, centered around launch. A comparison of ascent and descent electron density profiles for this rocket (not shown) also displays large spatial differences at that time. In contrast, Fig. 4 shows that for the other two rockets there is in general quite good agreement between ascent and descent results. In Fig. 7b, the agreement
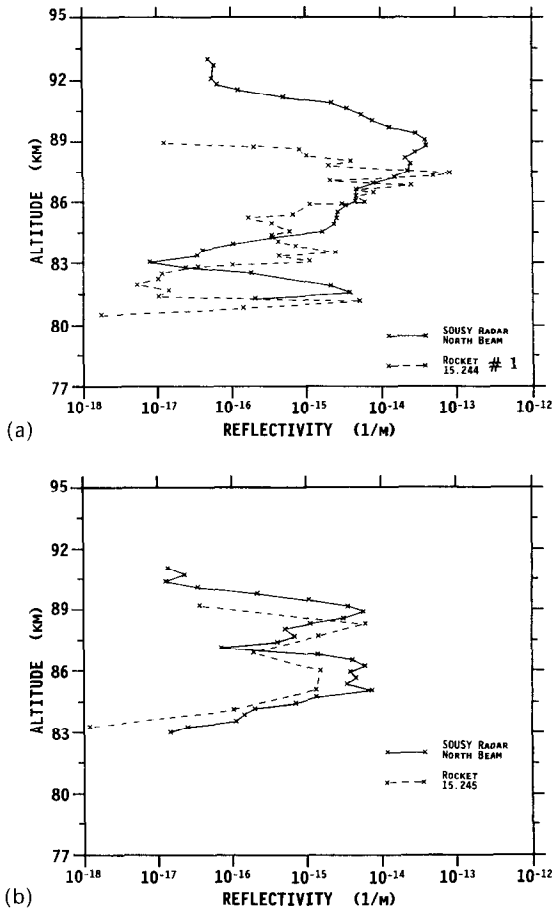
Fig. 7. Height profiles of the reflectivity η_{radar} $(\theta_0 = 5.6°)$ observed by the SOUSY radar in the northward beam and the reflectivity η_{rocket} estimated from simultaneous rocket observations under the assumption of isotropy. The plots (a) and (b) show the results for rocket flights No. 1 and 2 of the TGW salvo, respectively.

between the rocket and radar reflectivities is much better, each showing two regions of nearly the same intensity with a minimum near 87 km. However, a radar reflectivity systematically larger than that calculated from the rocket observations cannot be denied also for this second rocket flight, at least for heights below 87 km.

In both the above cases the rocket reflectivity calculation usually yields smaller values than those from the radar observations by 5–10 dB, which is contrary to what was found in the STATE experiments. In the latter case the off-zenith angle of the radar beam, however, was much larger than in the present experiment. A radar reflectivity slightly larger than the

reflectivity calculated from the rocket measurements was also observed during the EISCAT salvo even though the reflectivities found on that day were more than an order of magnitude larger than during the TGW salvo (KELLEY *et al.*, 1990). As pointed out earlier, the electron density for the EISCAT day was more than an order of magnitude greater than those measured during the TGW salvo in the structured regions.

3.3. Radar aspect sensitivity

During the first two launches, the echo intensity was large enough to determine the variability of the echo intensity with the off-zenith angle θ_0 of the radar beam. For this purpose, the reflectivity $\eta_{radar}(\theta_0)$ seen in all six radar beams was mapped into the height that corresponds to the observed range times $\cos\theta_0$. For each height gate and time record the reflectivities from the six beam directions were subsequently fitted to a Gaussian model angular dependence, or equivalently to

$$10\log\eta_{radar}(\theta_0) = \bar{\eta} + c\theta_0^2. \qquad (4)$$

Each of the fits yields estimates for the two model parameters, the vertical reflectivity $\bar{\eta}$ averaged over the six radar volume elements of the individual beams and the curvature c (in units of $dB/degree^2$), which is a measure of the aspect sensitivity. A similar model has been used by HOCKING *et al.* (1986) and CZECHOWSKY *et al.* (1988) to find the aspect sensitivity of their observations. In order to reduce random and systematic errors in the estimation of the two model parameters, they were only accepted if η_{radar} exceeded a threshold value of $3 \cdot 10^{-17} m^{-1}$ for each beam, and was larger than at least 10^{-4} times the maximum η_{radar} of the height profile for each beam at that time. In this way, interference from side lobes of the antenna could be excluded. Another source of error is the unprecise height determination which leads to wrong estimates of c if $|d\eta_{radar}/dz|$ is large. Therefore, c was only determined when in addition to the above constraint η_{radar} changed with height more slowly than 8 dB/km in each beam.

In Fig. 8, we show the height profiles of the curvature c thus determined at the time of the first two rocket launches. For the first rocket, an averaging over 10 min was sufficient to obtain a continuous profile of c; for the second rocket 60-min averaging was necessary. At the time of the third launch, the echo power was too small for the analysis to yield reliable estimates of c. The width of the grey-shaded region in each panel of Fig. 8 represents the uncertainty of the estimated value of c due to the error
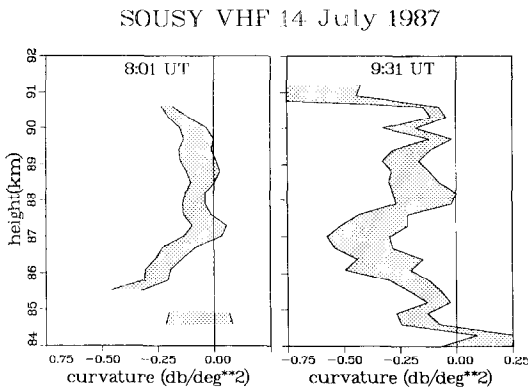
SOUSY VHF 14 July 1987

Fig. 8. Aspect sensitivity of the reflectivity during flight 1 and 2. For a definition of the curvature c see equation (4) and the adjacent text.

between the observed and model reflectivity of equation (4) : a variation of c within the given error bounds enhances the mean-square error of the fit to equation (4) by a factor $\leqslant 2$ relative to the least mean-square error. At both times in Fig. 8 we obviously find a clearly negative value for c, which indicates an anisotropic spectrum of the electron density fluctuations with the horizontal coherence length exceeding the vertical. The values for c are typically in the range between -0.5 and 0.0 dB/degree^2, which in order of magnitude coincides with earlier mesospheric VHF observations (CZECHOWSKY et al., 1988). A glance at the time variation of c shows that Fig. 8 is representative for the observations on the TGW day, while for the EISCAT day, when the backscatter was generally higher, no significant deviation of c from zero could be detected (KELLEY et al., 1990). HOCKING et al. (1986) have shown that the parameter c not only depends on the aspect sensitivity of the scattering medium, but is still contaminated by the antenna characteristic. A discussion of the unfolding of the antenna pattern and the intrinsic anisotropy of the scattering medium will be postponed until the next section, where it will be shown that the anisotropy is consistent with the observed underestimation of the radar reflectivity from the rocket observations.

4. IMPLICATIONS OF AN ANISOTROPIC TURBULENCE

The radar backscatter and the rocket probe are sensitive to different integrals over the spectral density $\phi_N(\mathbf{k})$ of the electron density irregularities δN_e. TATARSKII (1961) and OTTERSTEN (1969) pointed out that the power spectral density (3) derived from the rocket observations corresponds to a reduced, one-

dimensional power spectrum of the density irregularities:

$$S_N(k_\parallel) = 2 \int_{-\infty}^{\infty} d^2 k_\perp \phi_N(\mathbf{k}_\perp, k_\parallel). \tag{5}$$

Here, $k_\parallel$ and $\mathbf{k}_\perp$ are the wave number components parallel and perpendicular to the rocket velocity $\mathbf{V}$, respectively. Note that S_N and ϕ_N are normalized such that

$$\int_{-\infty}^{\infty} d^2 k_\perp \, dk_\parallel \phi_N = \int_0^\infty dk_\parallel S_N = \langle \delta N_e^2 \rangle$$

is equal to the mean-square of the density fluctuations. On the other hand, the radar reflectivity for an ideal antenna and for volume-filled scattering only depends on the spectral density very close to the single wave vector $\mathbf{k} = k\hat{n}_0$ where $k = 2k_{\text{radar}}$ and $\hat{n}_0$ is the direction of the antenna beam (OTTERSTEN, 1969):

$$\eta_{\text{radar}} = 32\pi^4 r_e^2 \phi_N(k\hat{n}_0). \tag{6}$$

Note that ϕ_N is related to the spectrum ϕ_n of the refractive index through

$$4\phi_n = (4\pi r_e/k_{\text{radar}}^2)^2 \phi_N = (\omega_p^2/N_e \omega_{\text{radar}}^2)^2 \phi_N$$

where ω_p and ω_{radar} are the plasma and the radar transmission frequency, respectively (WOODMAN and GUILLEN, 1974). For a finite beam width of the antenna system, ϕ_N in (6) has to be replaced by an appropriate angular average. With $g(\hat{n})$ being the antenna characteristic in direction $\hat{n}$ for the monostatic radar system, we have instead of (6)

$$\eta_{\text{radar}} = 32\pi^4 r_e^2 \frac{\int d\Omega \phi_N(k\hat{n}) g^2(\hat{n})}{\int d\Omega g^2(\hat{n})} \tag{7}$$

and the solid angle integration is to be performed over the angles of $\hat{n}$. For example, $\int d\Omega g(\hat{n}) = 4\pi/G$ is the beam solid angle and for a Gaussian beam shape that we shall assume here. Then the denominator in (7) just yields half the solid angle $2\pi/G$. Equations (5) and (7) integrate ϕ_N over different surfaces in k-space. A comparison of the integrals can, in the reverse, give information about the variation of the integrand ϕ_N.

In the Appendix, we derive a relation between (2) or (5) on the one hand and (7) on the other under the assumption that ϕ_N can be represented by an anisotropic spectral density of the form

$$\phi_N(\mathbf{k}) = \frac{C}{[k_z^2 + \alpha(k_x^2 + k_y^2)]^{q/2}}. \tag{8}$$

For an isotropic Kolmogoroff-spectrum, $q = 11/3$,

and if additionally N_e is an ideal passive tracer, then C is 0.033 times the structure constant C_N^2 (TATARSKII, 1961). Note that for a power law spectrum like (8), the spectral indices n of S_N and q of ϕ_N are related by $n = q - 2$. The parameter α is the square of the ratio of the horizontal to the vertical coherence length of the N_e fluctuations. We shall take this parameter as our measure of the spectral anisotropy. WOODMAN and CHU (1989) have pointed out that a unique anisotropy parameter α probably does not exist for realistic spectral densities ϕ_N, and that very probably the anisotropy decreases from a value very much larger than unity at the buoyancy wave number towards isotropy somewhere close to the viscous subrange. We need the model (8), however, only in the integrals (5) and (7) where (8) may be a valid approximation. With respect to real spectra, α therefore represents the ellipticity of the contour $\phi_N = \text{const}$ through $\mathbf{k} \simeq 2\mathbf{k}_{\text{radar}} \hat{n}_0$. For $\alpha = 1$, these contour surfaces are concentric spheres; for $\alpha > 1$ they become cigar-shaped and for $0 \leqslant \alpha < 1$ the contours are pancake-like. The case $\alpha = 1$ corresponds to isotropic scattering while in the limit $\alpha \to \infty$ we have Fresnel scatter.

The relation between equations (2), (5) and (7) derived in (A7) in the Appendix is

$$\eta_{\text{radar}}(\theta_0 = 0) = 8\pi^3 \left(\frac{r_e}{k}\right)^2 (q-2) f_1 f_2 S_N(k)$$

$$= f_1 f_2 \eta_{\text{rocket}}(k) \qquad (9)$$

where

$$f_1 = \frac{\alpha}{1 + (\alpha - 1)q/G}$$

yields the correction due to a finite antenna beam width in case of anisotropy, while

$$f_2 = \left(\frac{1 + (\alpha - 1)\cos^2\theta_\parallel}{\alpha}\right)^{(3-q)/2}$$

takes account of a possible deviation of the rocket path from the vertical by an angle $\theta_\parallel$. For isotropic scattering ($\alpha = 1$) both f_1 and f_2 are unity and (9) corresponds to the formula employed by ROYRVIK and SMITH (1984), or in view of (2), $\eta_{\text{radar}} = \eta_{\text{rocket}}$. In the limit of Fresnel scatter, $\alpha \to \infty$, we recover the scattering formula given by GAGE et al. (1985), as discussed in the Appendix.

Since $n = q - 2$ is the spectral index of the one-dimensional spectrum S_N, relation (9) can be used to infer the only unknown, the anisotropy parameter α. The rocket spectra in fact show that at SOUSY's wave number $q \simeq 11/3$ for a large part of the relevant height
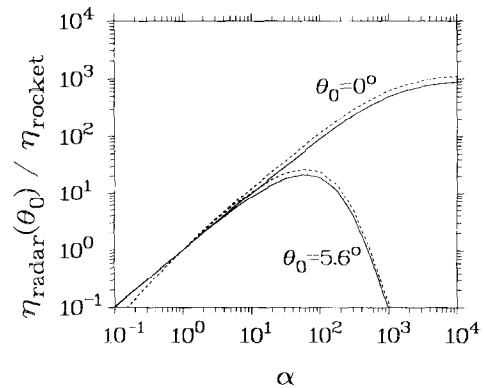

Fig. 9. Ratio of the radar reflectivity to the reflectivity determined from the rocket data as a function of the anisotropy parameter α. The curves are plotted for a rocket velocity off-zenith angle $\theta = 0°$ (solid) and $45°$ (dashed) and for a vertical $\theta_0 = 0°$ and an oblique radar beam with $\theta_0 = 5.6°$. A spectral index of the inertial range was assumed and the antenna parameters according to the SOUSY radar.

range. In Fig. 9 the product of f_1 and f_2 or likewise, the ratio of $\eta_{\text{radar}}(\theta_0 = 0)$ over η_{rocket} is plotted by the graphs labeled $\theta_0 = 0$ as function of α for two angles $\theta_\parallel$ and for the antenna gain of the SOUSY radar. Clearly, the rocket inclination angle has relatively little impact compared to the anisotropy parameter α. In our case, the rocket off-zenith angle in 85 km was about $30°$ and its influence is negligible.

The anisotropy of the electron density fluctuations at $2k_{\text{radar}}$ can also be derived from the aspect angle variation of the radar reflectivity. HOCKING et al. (1986) have shown how the observed aspect angle dependence of η_{radar} is related to an intrinsic aspect angle dependence of the scattering structures and the radar beam width. The relation

$$\frac{1}{\eta_{\text{radar}}} \frac{d}{d\sin^2\theta_0} \eta_{\text{radar}} \bigg|_{\theta_0 = 0} = -\frac{(\alpha - 1)q/2}{1 + (\alpha - 1)q/G} \qquad (10)$$

derived in the Appendix in equation (A9) expresses furthermore the observed variation of η_{radar} with the off-zenith angle θ_0 of the antenna beam in terms of the spectral parameters α and q. With the help of (10), the anisotropy parameter α can be determined independently from (9), provided that again the spectral index q is known from rocket observations. The fact that the anisotropy changes the radar reflectivity in oblique radar beams has been taken account of in the second pair of graphs in Fig. 9 labeled $\theta_0 = 5.6°$, which is the zenith angle of the SOUSY northward beam. Again, the rocket velocity angle $\theta_\parallel$ has relatively little impact.

In the previous section we have seen that the radar

reflectivity observations indeed show a significant variation with θ_0, at least during the time of the TGW salvo. The relation between the observed curvature parameter c (see Fig. 8) and the left-hand side of (10) is, assuming $\sin \theta_0 \simeq \theta_0$,

$$\frac{1}{\eta_{\mathrm{radar}}} \frac{d}{d \sin^2 \theta_0} \eta_{\mathrm{radar}} \bigg|_{\theta_0 = 0} = \frac{\ln 10}{10 \sin^2 1^\circ} \cdot c \cong 756 \cdot c. \tag{11}$$

Since both sides of (10) are bounded by $\sim \frac{1}{2}q$ for $\alpha = 0$ and by $-\frac{1}{2}G$ for $\alpha \to \infty$, we therefore expect the curvature c to vary for the SOUSY radar between $-\frac{1}{2}G/756 = -2.35$ dB/degree^2 in the case of Fresnel scatter if $\alpha \to \infty$ and a value closely above zero if $\alpha \lesssim 1$. The observations in Fig. 8 lie well within these theoretical boundaries. Conversely, a typically observed value $c \cong -0.25$ dB/degree^2 yields an anisotropy parameter according to (10) and (11) of $\alpha \simeq 100$ if $q = 11/3$ is assumed. Note that for this value of α the denominator in (10) deviates from unity by only 10% for the SOUSY radar antenna so that the antenna characteristic is still negligible in our case. If we take it into account, a slightly larger value of α results. This estimate for α is unexpectedly large, implying that the horizontal coherence length is about 10 times larger than the vertical coherence length, if the ϕ_N contour surfaces were geometrically similar for all scales.

The observed curvature is also approximately consistent with the observed discrepancy between the oblique radar reflectivity $\eta_{\mathrm{radar}}(\theta_0 = 5.6^\circ)$ and the equivalent reflectivity η_{rocket} calculated from the rocket data under the assumption of isotropic turbulence. During the first flight of the TGW salvo, the curvature in Fig. 8a has values between -0.25 and -0.1 dB/degree^2 over a large height range. These observations yield an α between about 40 and 100 if inserted into (10) and (11). From Fig. 9 we subsequently find that these values of α correspond to a ratio of η_{radar} $(\theta_0 = 5.6^\circ)/\eta_{\mathrm{rocket}}$ of slightly larger than 10. This is indeed what we observe in Fig. 7a over a large portion of the rocket ascent trajectory through the echo layer, except perhaps near the peak of the layer where the reflectivity ratio approaches unity and the anisotropy seems to be only marginal. In the curvature observations, this feature might have been smoothed out due to the long averaging process. For the second flight, the curvature in Fig. 8b is generally larger in magnitude, in some heights even well below -0.25 dB/degree^2, which yields an α in excess of 100. From Fig. 9 we can see that the reflectivity ratio between radar and rocket observations rapidly declines for $\alpha \geqslant 100$ and $\theta_0 = 5.6^\circ$. The generally better agreement

between η_{radar} and η_{rocket} observed in this flight (Fig. 7b) seems plausible on these grounds, even though details of the height profiles cannot be explained.

To gain further perspective on this issue, we have plotted in Fig. 10a,b a family of curves representing scattering cross-sections as a function of zenith angle for different values of α and for the inertial and diffusive subranges, respectively. The curves are based on the fluctuation spectrum model (8). Included in the figures are vertical bars representing the scattering cross-sections that CZECHOWSKY *et al.* (1988) have deduced from their radar observations of polar mesospheric summer echoes. These are the only mesospheric observations so far that extend to large zenith angles of almost 40°. The darkest line corresponds to a Gaussian fit $\exp(-\sin^2 \theta/\sin^2 \theta_s)$ of the data bars at small angles. The e-folding angle θ_s has been given by CZECHOWSKY *et al.* (1988) as 5.44°. Their observations of small angles are also consistent with our model for a value of α of about 70 if a spectral index of $q = 11/3$, i.e. $n = 5/3$, is assumed. This value for the anisotropy is of the same order of magnitude as for the observations during the TGW day.

The Gaussian model of the scattering cross-section as a function of zenith angle has been proposed by HOCKING *et al.* (1986). Obviously, this model underestimates by far the observations at larger angles near 40°. Our model spectrum (8) yields cross-sections much closer to the large angle observations, yet it is still not totally consistent with the observations of CZECHOWSKY *et al.* (1988) because there is no unique value for α explaining the data at small and large angles within the given error bounds. When we consider the large angle data of CZECHOWSKY *et al.* (1988), a value for α only half as large as for the small angle fit is indicated.

The situation is even more extreme if we assume that the SOUSY wavelength was in the diffusive subrange. This is shown in Fig. 10b. Again the quasi-specular curve fits the low angle data but at large angles a value of $\alpha = 7$ matches the observations. Rocket data from the present and previous experiments show that the 3-m wavelength can be on either side of the break in the spectrum depending on the level of turbulence and the value of the Schmidt number (ULWICK *et al.*, 1988; KELLEY and ULWICK, 1988).

There are several possible solutions to this difference. It may be that quasi-specular reflections dominate the near-vertical scattering and that turbulent processes act at large off-vertical angles. In very strongly turbulent situations as described, for example, by KELLEY *et al.* (1990), turbulent processes may also mask the quasi-specular reflection in the vertical observations. As another possibility, physics
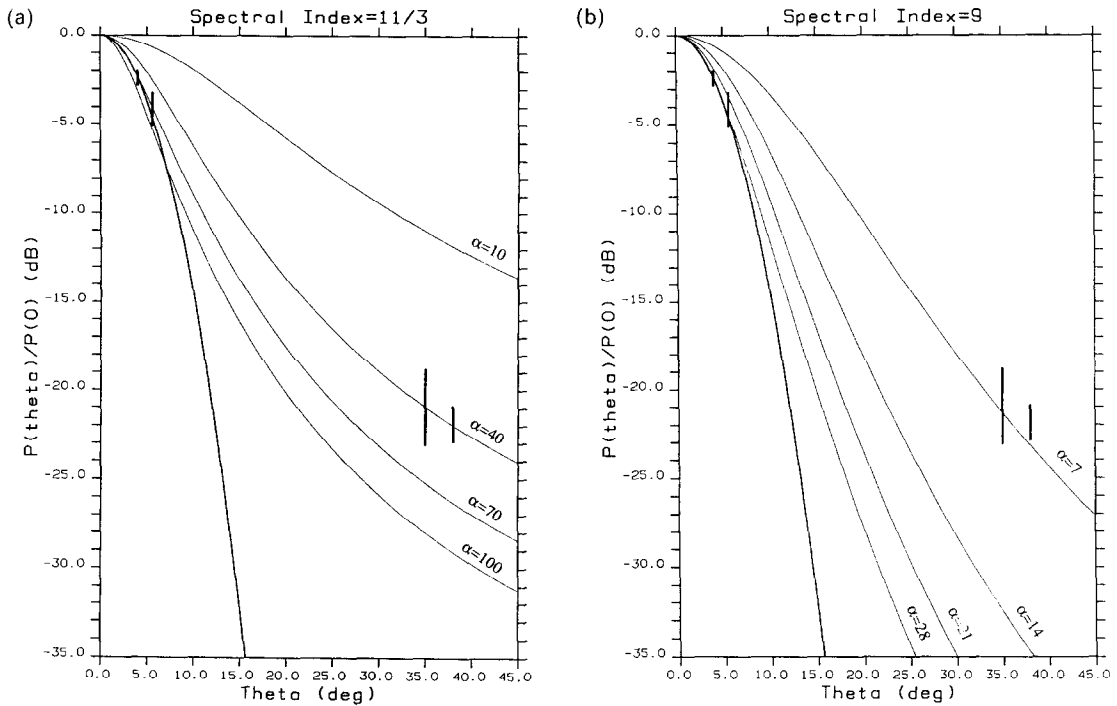
(a)

(b)

Fig. 10. The relative cross-section with zenith angle θ for the anisotropic power law model (8) for various anisotropy parameters α in the inertial (a) and diffusive (b) subrange. Note that the spectral indices of $11/3$ and 9 of the three-dimensional spectral density correspond to the indices $5/3$ and 7, respectively, for the energy spectral density average over all angles. The vertical bars are cross-section observations of CZECHOWSKY *et al.* (1988). The heavy line is a Gaussian fit to the data according to HOCKING *et al.* (1986).

may dictate a slight modification to the functional form of the fluctuation spectrum model (8). It is likely that the spectral slope of the fluctuation spectrum depends on the zenith angle. Given highly anisotropic gravity wave turbulence at small wave numbers and gradual isotropization towards large wave numbers, the resultant slope of the spectral energy cascade would be less steep at large zenith angles than in the vertical direction. Since more gentle slopes yield less aspect sensitivity with our model (compare Fig. 10a and b), this could account for the apparent decrease in aspect sensitivity of the data at larger angles.

5. SUMMARY AND DISCUSSION

Both the variation of the radar reflectivity with zenith angle and the radar–rocket reflectivity comparison are in good agreement with the presence of an anisotropic turbulence in the mesosphere during the observations on the TGW day. An exact quantitative consistency cannot be expected because the measurements in the mesosphere are far from ideal: the rocket picks out a single density profile along its trajectory, whereas good statistics would be required for the estimate of turbulence parameters; the radar data are interpreted as if the turbulence were homogeneous over the radar volume of more than 3 km^3, which is probably not the case. Furthermore, the rocket trajectory and the radar volume were about 24 km apart, which certainly can make a difference on the scale of the radar wavelength of about 3 m. Note, however, that the comparison in Fig. 4 of the ascent and descent rocket results shows some surprising similarities in the electron density at medium-scale sizes of some kilometers over a horizontal distance of some 10 km. Both methods yield on average for the TGW day a ratio for the square of the horizontal to the vertical coherence length of about 100. This result coincides with earlier observations of CZECHOWSKY *et al.* (1988) if they are re-interpreted with our model. However, there are also radar observations which show that occasionally the scattering irregularities in the summer polar mesosphere may be almost isotropic (KELLEY *et al.*, 1990).

We note here that the errors which enter into the estimation of the radar aspect sensitivity are con-

siderable. This is probably again due to the lack of homogeneity of the turbulence over the distance between the volumes illuminated by the different radar beams. From Fig. 8 it seems that a typical resolution for the estimate of the curvature parameter c is about 0.1 dB/degree^2. This corresponds to a value of $\alpha \cong 40$. The variation of the radar reflectivity with zenith angle is therefore not a very sensitive method to observe the turbulent anisotropy in the mesosphere. Anisotropy ratios of $\alpha \leqslant 10$ may well remain unresolved by a radar. On the other hand, we estimate the calibration errors of the radar and rocket probe together to be smaller than a factor of 10, so that the comparison of the radar and rocket reflectivities can give more reliable estimates of the anisotropy when the radar beam and the rocket trajectory are in close vicinity.

Our interpretation of the TGW day observations also casts some new light on similar measurements during the STATE campaign that have been reported by ULWICK et al. (1988). In contrast to our observations, in their case the equivalent reflectivity estimated from the rocket results were systematically larger than those seen by the radar, sometimes almost by a factor of 10. This can be explained by the presence of a comparably moderate anisotropy with a squared coherence length ratio of $\alpha \simeq 40$. In the vertical beam, η_{radar} would then exceed η_{rocket} by a factor of about 40, but for the 15° off-zenith beam used for the comparison, η_{radar} would be depleted by $10^{-22.5c}$ with respect to the vertical. The above α corresponds to $c \simeq -0.1$ dB/degree^2 for a radar similar to SOUSY and for observations inside the inertial range. In all, this yields a value for η_{radar} in the oblique beam about a factor 5 less than η_{rocket}.

The profiles of the observed anisotropy, or likewise the curvature (see Fig. 8), show an appreciable variation with height. Since the molecular diffusion and hence the Kolmogoroff micro-scale steadily increases with height, one might expect the anisotropy to gradually decrease with height and the curvature c to approach zero. In our observations, we cannot see this tendency and a reason for this could be the fact that it is not the diffusion of the ions that isotropizes the density fluctuation but rather the local strength of the turbulence energy.

Our observations seem to indicate a weak anticorrelation of the anisotropy with the radar reflectivity: the curvature c has a tendency to come close to zero at the height where the reflectivity has a maximum and it is in these heights where the discrepancy between η_{radar} and η_{rocket}, and hence the anisotropy, is smallest. This tendency is supported by the variation of the curvature in time: while the radar echo power clearly decreases between the launch of

the first and second rocket, the curvature increases in magnitude and so does the anisotropy. Furthermore, the observations one day later, on the EISCAT day (KELLEY et al., 1990), show much higher reflectivities than on the TGW day and a curvature of about zero within the error bounds. As far as we can conclude from our limited data, there is an even closer anticorrelation of the anisotropy with the spectral width of the radar signals. Comparing Figs 6 and 8, it is obvious that the strong anisotropy in 87 km at 0931 UT is associated with a small backscatter signal width. Near 89 km the vertical fluctuations are much broader at both 8 and 0930 UT and the anisotropy is only moderate at that height. A similar anti-correlation between the aspect sensitivity and the spectral width of backscatter from the polar summer mesopause has recently been noted by CZECHOWSKY et al. (1988).

The most probable source of the anisotropy at the radar wave number is the large anisotropy of gravity waves at scales of several hundreds of meters and more. Typically, the horizontal velocity fluctuations at these scales are an order of magnitude larger than the vertical fluctuations (SMITH et al., 1985). The anisotropy parameter α at these large scales could, to a first approximation, be equated to the ratio of the horizontal over the vertical kinetic energy, i.e. $\alpha \geqslant 10^2$ in the buoyancy subrange. The good correspondence of the electron density variations at a vertical scale of some kilometers between the ascent and descent of the Super ARCAS rockets trajectory supports this estimate for the anisotropy at these large scales. The associated anisotropic velocity fluctuations drive more or less continuously the turbulence in the inertial subrange from its lower wave number end. The rate at which energy is fed into the inertial subrange is about ε, the rate at which the energy leaves the inertial subrange again into the viscous subrange. In a somewhat simplified picture, the action exerted by the buoyancy subrange fluctuations onto the inertial subrange can probably be considered equivalent to the excitation of turbulence by a highly anisotropic driving force at small wave numbers. While the energy thus imposed is cascaded by nonlinear forces through the inertial subrange to smaller scales, these forces also tend to randomize the velocity fluctuations in direction and thereby isotropize the fluctuation spectrum towards the larger wave numbers. Opposed to this, gravity will try to maintain the anisotropy because the energy of the vertical motion is partly absorbed by potential energy. For an eddy of size $2\pi/k$ the necessary potential energy per volume element is about $\rho\omega_B^2 k^{-2}$, where ω_B is the Brunt–Väisälä frequency. However, in the inertial subrange this energy is much smaller than the available kinetic
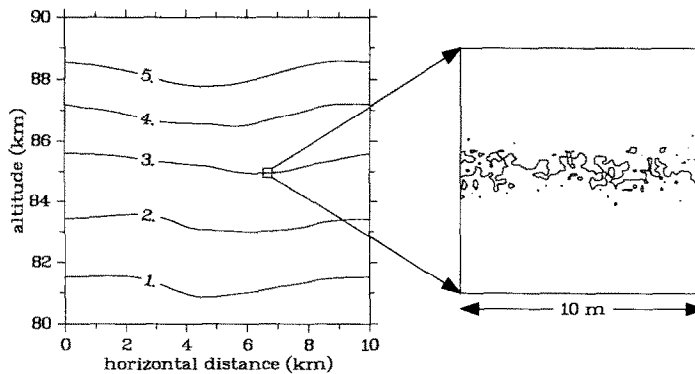
Fig. 11. Hypothetical electron density contour lines in the mesosphere. When switching from scales far above the buoyancy wavelength of some 100 m to much smaller scales, the density contour lines exhibit a fine-structure due to the excess of turbulent kinetic energy at the small scales.

energy ρv_k^2 of the eddy if a Kolmogoroff spectrum $E_k = v_k^2/k \simeq \varepsilon^{2/3}k^{-5/3}$ is assumed. The wave number at which the kinetic and the potential energies become about equal is the buoyancy wave number (WEIN-STOCK, 1985)

$$k_B = (\omega_B^3/\varepsilon)^{1/2} \qquad (12)$$

which defines the low wave number end of the inertial subrange. Well above k_B, gravity therefore becomes a negligibly small ingredient to the equation of motion and the neutral air behaves very much like a Navier–Stokes fluid. Hence, in the inertial subrange, we expect the nonlinear forces to dominate gravity and accordingly a gradual isotropization of the fluctuation spectrum should occur towards larger wave numbers.

At the moment, we cannot say quantitatively how efficiently we expect this isotropization to work. If the turbulence level is sufficiently small it is quite possible that a complete isotropization may not yet be achieved at the upper end of the inertial subrange and the turbulence might still maintain a residual anisotropy in the viscous subrange. Roughly, the distance in k-space between the radar wave number and the buoyancy wave number could be taken as a measure of how much isotropization of the turbulent energy can be obtained while it is cascaded through the inertial subrange at a flux rate ε. From (12) we observe that with increasing ε the buoyancy wave number decreases and therefore moves away from the radar wave number. Since ε is most likely positively correlated with the vertical velocity fluctuations (WEIN-STOCK, 1981), this could qualitatively explain the observed decrease of the anisotropy at the radar wave number when the turbulent velocity fluctuations or the reflectivity are enhanced.

The above scenario tacitly assumes that the radar

echoes are due to scattering from anisotropic turbulence. Quasi-specular reflection is often considered as an alternative scattering mechanism. A necessary condition for quasi-specular reflection is the existence of relatively smooth and layered contour levels of the electron density near the scale $2\pi/k_{radar}$ of the radar wavelength. As stated above, however, eddies with a wave number $k > k_B$ have more kinetic energy than they need to lift a volume element of the neutral air over the eddy size $2\pi/k$. We therefore expect the excess of kinetic energy to destroy any initial stratification at these scales. In Fig. 11, for example, we illustrate the resulting break of self-similarity of the electron density contour lines between scales larger and smaller than $2\pi/k_B$ due to the expected imbalance of kinetic and potential energies. For specular reflection conditions to be present, the buoyancy wave number k_B must consequently increase to be of the order of the radar wave number k_{radar}. If the SOUSY radar wave number is inserted into (12) and ε is equated to $0.4\omega_B\sigma^2$ (WEINSTOCK, 1981), a spectral variance of only $\sigma^2 \simeq 10^{-4}$ m^2/s^2 results. In view of the observed variance of the vertical fluctuations of $\sigma^2 > 1$ m^2/s^2, it seems unlikely that the mesosphere is so calm as to maintain a layering of the electron density contours at this scale. We note, however, that the observed spectra may be broadened by the effect of a horizontal wind shear or the finite beam width of the radar (HOCKING, 1983). The effect of a stratification at larger scales can probably still be felt at the radar wavelength as it might induce an anisotropy in the turbulent fluctuations as discussed above. In this sense, quasi-specular reflection can be considered as the limiting case of anisotropic turbulent scatter in which the distance in k-space between the radar and the buoyancy wave number shrinks to zero. The

enhanced radar returns when approaching the quasi-specular reflection limit are due to the enhanced horizontal coherence length which in our description is parameterized by α. A shortcoming of our model (8) for the fluctuation power spectral density which in the end defines α is that it has been chosen purely empirically. Whether it is a physically realistic model deserves future investigations.

Another open question concerns the nature of echo layers as they were observed during the second flight on TGW day around 85 km and also by CZECHOWSKY et al. (1988). Their signature is a large anisotropy and a small turbulence level in accordance with the above discussion. They also seem to be associated with an anomalously strong radar backscatter and with a deep 'bite-out' in the vertical electron density profile. The different response of the d.c. and RF rocket probe inside the 'bite-out' region raises the suspicion that chemical processes are active that may also be responsible for the enhanced radar backscatter.

REFERENCES

ABRAMOWITZ M. and STEGUN I. A.	1964	*Handbook of Mathematical Functions*. National Bureau of Standards, Washington, D.C.
BAKER K. D., LABELLE J., PFAFF R. F., HOWLETT L. C., RAO N. B., ULWICK J. C. and KELLEY M. C.	1985	*J. atmos. terr. Phys.* **47**, 781.
BAKER K. D. and ULWICK J. C.	1978	*J. geophys. Res.* **5**, 723.
BATTAN L. J.	1973	*Radar Observations in the Atmosphere*. The University of Chicago Press, Chicago.
CZECHOWSKY P., REID I. M. and RÜSTER R.	1988	*Geophys. Res. Lett.* **15**, 1259.
CZECHOWSKY P., SCHMIDT G. and RÜSTER R.	1984	*Radio Sci.* **19**, 441.
FRITTS D. C., SMITH S. A., BALSLEY B. B. and PHILBRICK C. R.	1988	*J. geophys. Res.* **93**, 7015.
FUKAO S., SATO T., KATO S., HARPER R. M., WOODMAN R. F. and GORDON W. E	1979	*J. geophys. Res.* **84**, 4379.
GAGE K. S., ECKLUND W. L. and BALSLEY B. B.	1985	*Radio Sci.* **20**, 1493.
HARRIS R., HOWLETT L. C. and BAKER K. D.	1983	*J. atmos. terr. Phys.* **45**, 437.
HILL R. J. and BOWHILL S. A.	1976	*Aeronomy Rep.* **75**, 261.
HOCKING W. K.	1983	*J. atmos. terr. Phys.* **45**, 89.
HOCKING W. K., RÜSTER R. and CZECHOWSKY P.	1986	*J. atmos. terr. Phys.* **48**, 131.
HOCKING W. K., SCHMIDT G. and CZECHOWSKY P.	1983	Absolute calibration of the SOUSY VHF stationary radar. Max-Planck-Institut für Aeronomie Report, MPAE-W-00-83-14, Katlenburg-Lindau, F.R.G.
HOCKING W. K. and VINCENT R. A.	1982	*J. atmos. terr. Phys.* **44**, 843.
KELLEY M. C., FARLEY D. T. and RÖTTGER J.	1987	*Geophys. Res. Lett.* **14**, 1031.
KELLEY M. C., PFAFF R., BAKER K. D., ULWICK J. C., LIVINGSTON R., RINO C. and TSUNODA R.	1982	*J. geophys. Res.* **87**, 1575.
KELLEY M. C. and ULWICK J. C.	1988	*J. geophys. Res.* **93**, 7001.
KELLEY M. C., ULWICK J. C., RÖTTGER J., INHESTER B., HALL T. and BLIX T.	1990	*J. atmos. terr. Phys.* **52**, 875.
OTTERSTEN H.	1969	*Radio Sci.* **4**, 1251.
PFAFF R. F., KELLEY M. C., FEJER B. G., MAYNARD N. C. and BAKER K. D.	1982	*Geophys. Res. Lett.* **9**, 688.
PRAKASH S., SUBBARAYA B. H. and GUPTA S.	1972	*Indian Radio Space Phys.* **1**, 72.
REID G. C.	1989	*J. geophys. Res.* **94**, 653.
ROYRVIK O.	1985	*Radio Sci.* **20**, 1423.
ROYRVIK O. and SMITH L. G.	1984	*J. geophys. Res.* **89**, 9014.
SMITH A. S., FRITTS D. C. and VAN ZANDT T. E.	1985	*Radio Sci.* **20**, 1331.
SZUSZCZEWICZ E. P., TSUNODA R. T., NARCISI R. and HOLMES J. C.	1980	*Geophys. Res. Lett.* **7**, 537.
TATARSKII V. I.	1961	*Wave Propagation in a Turbulent Medium*. Dover Publications, New York.
THRANE E. V. and GRANDAL B.	1981	*J. atmos. terr. Phys.* **43**, 179.

THRANE E. V., GRANDAL B., FLA T. and BREKKE A.   1981   *Nature* **292**, 221.
ULWICK J. C., BAKER K. D., KELLEY M. C.,   1988   *J. geophys. Res.* **93**, 6989.
   BALSLEY B. B. and ECKLUND W. L.
WEINSTOCK J.   1981   *J. atmos. Sci.* **38**, 880.
WEINSTOCK J.   1985   *Radio Sci.* **20**, 1295.
WOODMAN R. F. and CHU Y.-H.   1989   *Radio Sci.* **24**, 113.
WOODMAN R. F. and GUILLEN A.   1974   *J. atmos. Sci.* **31**, 493.

APPENDIX

In the reference frame of the rocket, an orthogonal basis for the wave number space is given by $k_{\parallel}, k_{\perp}, k_y$, where $k_{\parallel}$ is the component along the rockets' velocity $\mathbf{V}$ and in the horizontal plane, k_y is perpendicular to $\mathbf{V}$ and in the horizontal plane, $k_{\perp}$ is perpendicular to both $\mathbf{V}$ and $\hat{y}$. In this coordinate system, (8) can be written as

$$\phi_N(\mathbf{k}) = C \cdot [\alpha k^2 + (1-\alpha)k_z^2]^{-q/2}$$

$$= C \cdot \left[\frac{\alpha}{\beta}k_{\parallel}^2 + s_{\perp}^2 + s_y^2\right]^{-q/2} \quad \text{(A1)}$$

where

$$s_{\perp} = \sqrt{\beta}k_{\perp} - (1-\alpha)k_{\parallel}\cos\theta_{\parallel}\sin\theta_{\parallel}/\sqrt{\beta}$$

$$s_y = \sqrt{\alpha}k_y$$

$$\beta = \alpha + (1-\alpha)\sin^2\theta_{\parallel}$$

and $\theta_{\parallel}$ is the angle beam between $\mathbf{V}$ and the vertical. Insertion of (A1) into (5) yields, after a transformation of the integration variables $k_{\perp}, k_y$ to $s_{\perp}, s_y$

$$S_N(k_{\parallel}) = \frac{2C}{\sqrt{\alpha\beta}}\int d^2s\left(\frac{\alpha}{\beta}k_{\parallel}^2 + s^2\right)^{-q/2}$$

$$= \frac{4\pi}{q-2}\frac{\beta^{(q-3)/2}}{\alpha^{(q-1)/2}}\frac{C}{k_{\parallel}^{q-2}}. \quad \text{(A2)}$$

It is essentially β that gives rise to the correction factor f_2 in equation (9).

In order to integrate (7), we assume a Gaussian antenna beam with a characteristic

$$g(\hat{n}) = \exp\left(-\tfrac{1}{4}G\sin^2\theta\right) \quad \text{(A3)}$$

where θ is the angle that $\hat{n}$ makes with the beam axis $\hat{n}_0$. Note that our normalization $\int d\Omega g(\hat{n}) = 4\pi/G$ is achieved if the approximation $\sin\theta \simeq \theta$ is made. For vertical incidence $\hat{n}_0 = \hat{z}$ the model spectral density (8) can in the integrand in the numerator of (7) be expressed as

$$\phi_N(k\hat{n}_0) = \frac{C}{k^q}[1 + (\alpha-1)\sin^2\theta]^{-q/2}.$$

The resulting integral (7) is straightforward and can be expressed in terms of the incomplete Γ-function if again the approximation $\sin\theta \simeq \theta$ is made. Note that the denominator in (7) gives $\int d\Omega g(\hat{n})^2 = 2\pi/G$, so that after a transformation of θ^2 to a new integration variable s

$$\eta_{\text{radar}}(\theta_0 = 0°) = 32\pi^4 r_e^2 \frac{C}{k^q}\frac{G}{2}\int_0^\infty ds\frac{\exp-(\tfrac{1}{2}Gs)}{[1+(\alpha-1)s]^{q/2}}. \quad \text{(A4)}$$

We abbreviate $x = \tfrac{1}{2}G/(\alpha-1)$ and further transform $1+(\alpha-1)s$ to a new variable t, which immediately yields

$$\eta_{\text{radar}}(\theta_0 = 0°) = 32\pi^4 r_e^2 \frac{C}{k^q}x^{q/2}e^x\Gamma\left(1-\frac{q}{2},x\right)$$

$$= 32\pi^4 r_e^2\frac{C}{k^q}x\left(\cfrac{1}{x+}\cfrac{\frac{q}{2}}{1+}\cfrac{1}{x+}\cfrac{1+\frac{q}{2}}{1+}\cdots\right) \quad \text{(A5)}$$

where in the last step we employed the continued fraction expansion of the incomplete Γ-function (ABRAMOWITZ and STEGUN, 1964). Unless the anisotropy parameter α is extremely large the argument x of the Γ-function is much greater than unity, so that only the first terms of the continued fraction are important. In this case,

$$\eta_{\text{radar}}(\theta_0 = 0°) \simeq 32\pi^4 r_e^2\frac{C}{k^q}\cdot\left[1+(\alpha-1)\frac{q}{G}\right]^{-1}. \quad \text{(A6)}$$

This result even holds as a reasonable approximation in the case of small x or a large anisotropy because the continued fraction has a limiting value $x/[(q/2)-1]$ for $x \to 0$, while in the above approximation a value of $x/(q/2)$ is obtained. This factor of $(q-2)/q$ by which (A6) is in error for very large α is tolerable in view of the model character of our calculations. Note that (A6) can be analytically continued to values $\alpha < 1$ even though the derivation is valid only for $\alpha \geqslant 1$. The usual isotropic scattering formula (6) is therefore applicable as long as $|\alpha-1| \ll G/q$. In the opposite case, i.e. if the horizontal coherence length exceeds the vertical coherence length appreciably, the reflectivity is dominated by Fresnel scatter.

A comparison between (A2) and (A6) yields

$$\eta_{\text{radar}}(\theta_0 = 0) = 8\pi^3\left(\frac{r_e}{k}\right)^2\frac{\alpha(q-2)}{1+(\alpha-1)q/G}$$

$$\times\left(\frac{1+(\alpha-1)\cos^2\theta_{\parallel}}{\alpha}\right)^{(3-q)/2}S_N(k). \quad \text{(A7)}$$

For $\alpha = 1$, we recover relation (6) of ROYRVIK and SMITH (1984) or $\eta_{\text{radar}} = \eta_{\text{rocket}}$. For an extremely anisotropic turbulence with $|\alpha-1| \gg G/q$ and $\theta_{\parallel} = 0°$, we obtain relation (4) of GAGE *et al.* (1985) except for the factor $(q-2)/q$ by which (A6) is in error for very large α as discussed above. To recover their relation we have to recall that $\eta_{\text{radar}} = 4\pi\sigma$ and the differential cross-section σ per volume element may be replaced by $r^2|\rho^2|/4$ in the radar equation in the case of Fresnel scatter, where $|\rho^2|$ is the reflection coefficient in at distance r. Note also that $\pi S_N(k_z)$ is equal to the Fourier transform of the vertical density acf.

For oblique incidence the resulting integration in (7) becomes very involved and can only be done numerically. In a spherical coordinate system oriented along the beam axis $\hat{n}_0$, the model spectral density can be written as

$$\phi_N(k\hat{n}) = \frac{C}{k^q}[\alpha + (1-\alpha)(\cos\theta\cos\theta_0 + \cos\phi\sin\theta\sin\theta_0)^2]^{-q/2}$$

where θ_0 is the zenith angle of the beam axis and θ and ϕ are the coordinates to be integrated over. We are,

however, mainly interested in an expression to be compared with the observed curvature which is essentially $d\eta_{radar}/d\sin^2\theta_0 = \frac{1}{2}d^2\eta_{radar}/d\theta_0^2$ at $\theta = 0°$. Since this differentiation and the integration can be interchanged, we end up with integrals similar to the one above:

$$-\left(32\pi^4 r_c^2 \frac{C}{k^q}\right)^{-1}\left(\frac{d}{d\theta_0}\right)^2 \eta_{radar}\Bigg|_{\theta_0=0}$$

$$= (\alpha-1)q\,\frac{G}{2}\int_0^\infty ds\left[\frac{1-\frac{3}{2}s}{[1+(\alpha-1)s]^{q/2+1}}\right.$$

$$\left.-\frac{(\alpha-1)\left(\frac{q}{2}+1\right)(s-s^2)}{[1+(\alpha-1)s]^{q/2+2}}\right]e^{-(1/2)Gs}$$

$$\simeq (\alpha-1)q\,\frac{G}{2}\Bigg[\left(1+\frac{3}{2}\frac{d}{d\left(\frac{G}{2}\right)}\right)\frac{1}{\left[\frac{G}{2}+(\alpha-1)\left(\frac{q}{2}+1\right)\right]}$$

$$+(\alpha-1)\left(\frac{q}{2}+1\right)\left(\frac{d}{d\left(\frac{G}{2}\right)}+\frac{d^2}{d\left(\frac{G}{2}\right)^2}\right)$$

$$\times\frac{1}{\left[\frac{G}{2}+(\alpha-1)\left(\frac{q}{2}+2\right)\right]}\Bigg]$$

$$\simeq \frac{(\alpha-1)q}{[1+(\alpha-1)(q+2)/G]^2}. \tag{A8}$$

In the last but one step, we made the same approximation as in (A6) and the very last equation holds when $G \gg 1$. Moreover, we neglected the slight difference between $q/2+2$ and $q/2+1$ because the terms involved only become important if $(\alpha-1)q/G$ becomes larger than unity, and in this case the approximation anyway bears a slight error of the same order as discussed above. Neglecting furthermore the difference between $q+2$ and q for the same reason, we obtain finally an expression for the aspect sensitivity for the nearly vertical radar beam

$$\frac{1}{\eta_{radar}}\frac{d}{d\sin^2\theta_0}\eta_{radar}\Bigg|_{\theta_0=0} = -\frac{(\alpha-1)q/2}{1+(\alpha-1)q/G}. \tag{A9}$$

For moderate values of α, i.e. for almost isotropic scatter, (A9) varies almost linearly with the square ratio of the coherence lengths. For $\alpha \to \infty$, the right-hand side of (A9) approaches $-G/2$ and the aspect angle variation is entirely determined by the square of the antenna characteristic (A3).